Fast atlas-based MRI-guided PET attenuation map generation in whole-body PET/MR imaging

Hossein Arabi and Habib Zaidi†, *Senior Member, IEEE*

***Abstract* – We propose a one registration multi atlas (ORMA) pseudo-CT generation algorithm for attenuation correction in whole-body PET/MRI based on an optimized atlas-guided bone segmentation procedure. The proposed approach requires only one online registration between the target and reference images regardless of the number of atlas images *N*, while for the remaining subjects belonging to the atlas dataset, the pre-computed transformation matrices obtained from registration to the reference image is used to align them to the target image. The performance characteristics of the proposed method were evaluated and compared to conventional atlas-based attenuation map generation consisting of direct registration of the entire atlas images to the target. Four different PET attenuation maps were produced using direct registration and ORMA, voxelwise weighted (VWW-Direct and VWW-ORMA) and arithmetic average (AA-Direct and AA-ORMA) atlas fusion strategies. The comparison of validation measures characterizing the accuracy of extracted whole-body bone demonstrated the superiority of VWW-Direct atlas fusion technique resulting in a Dice similarity measure of 0.82±0.04 compared to 0.60±0.02 for AA-Direct. Conversely, the ORMA approach yielded a Dice similarity measure of 0.76±0.05 for VWW-ORMA and 0.55±0.03 for AA-ORMA. Quantitative analysis of PET data revealed good correlation (y=1.01x+0.1, R^2=0.99) between PET images corrected for attenuation using the proposed pseudo-CT method and the corresponding reference CT images. The proposed method generates decent attenuation maps and enables to reduce the processing time for atlas-based pseudo-CT generation reduced by a factor *N*.**

I. Introduction

In previous work, we compared the performance of a variety of atlas-based segmentation methods for whole-body bone segmentation [1]. As a result, an optimized segmentation algorithm was devised which outperformed other methods for whole-body attenuation map generation in terms of bone extraction accuracy. One of the major challenges of atlas-based attenuation map generation methods is the long computation time taken by image registration. Depending on the number of atlas images, *N* registrations should be carried out to create one attenuation map [2]. The aim of this work is to propose a one registration multiple atlas (ORMA) pseudo-CT generation approach enabling to reduce drastically the computation time. The proposed approach requires only one online image registration for each target subject regardless of the number of atlas images and at the same time benefits from the information present in multiple atlas datasets. For the validation part, the performance of ORMA method was compared with direct registration of the entire atlas images to the target followed by non-weighting and voxel-wise weighting atlas fusion strategies. The resulting pseudo-CT images were evaluated in terms of accuracy of extracted bone through standard segmentation measures as well as quantitative assessment of tracer uptake in corresponding attenuation corrected PET images.

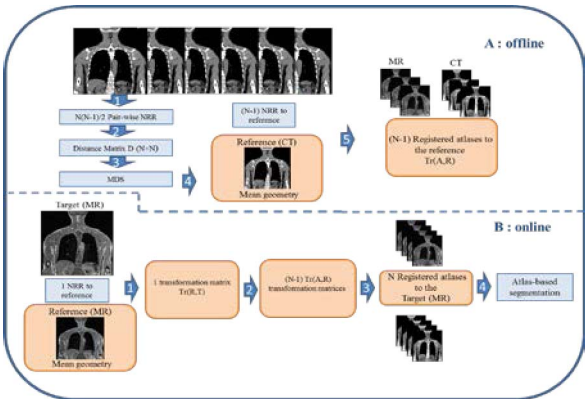

Fig 1. Schematic description of ORMA pseudo-CT generation approach.

II. Material and Methods

Clinical PET-CT-MRI studies

The study population comprised 23 patients who underwent PET-CT and PET-MRI examinations including acquisition of a low-dose CT for attenuation correction of the PET data and whole-body Dixon 3D volumetric interpolated T1-weighted MR sequence. All MR images were corrected by gradient anisotropic diffusion filter and N4 bias field correction [3] followed by inter-patient histogram matching.

ORMA pseudo-CT generation

Fig. 1 presents a schematic description of the ORMA pseudo-CT generation approach, which consists of offline and online steps. The first step of the ORMA pseudo-CT generation procedure is to determine the reference image representing the mean geometry of the patient population to minimize potential spatial deformation bias. The reference image should have a minimum sum of distances to other subjects in the atlas dataset. The distance between two images is defined based on the bending energy, which is the sum of squared second partial derivatives of the geometric distance [4]. To calculate the bending energy between two subjects [5] in the atlas data set, pair-wise alignment among all subjects in the atlas dataset was performed which represents $N(N-1)/2=253$ non-rigid registrations. The geometric distances obtained from pair-wise registrations are used to form a 23×23 distance matrix (D) (whose elements d_{ij} stand for the geometric distance between object i and j) [6]. The distance matrix was processed using multidimensional scaling (MDS) to

978-1-4673-9862-6/15/$31.00 ©2015 IEEE

determine the mean geometry of the population. The MDS produces a number of coordinates in a user defined dimension based on the Eigen structure of the distance matrix. We transformed the distance matrix D into two most meaningful coordinates computed by MDS where the closest subject to the origin represents the reference.

The matrix B is computed considering $B=1/2JD^{(2)}J$ using the matrix $J=I-N^{(-1)}\ 11'$, where N is the number of subjects, I is the identity matrix and $11'$ denotes a square matrix of ones. The two largest Eigenvalues λ_1 and λ_2 of B and the corresponding two Eigenvectors are extracted. A 2-D spatial configuration of the N objects is derived from the coordinate matrix $X = E_2\ C_2^{1/2}$, where E_2 is the matrix of 2 Eigenvectors and C_2 is the diagonal matrix of 2 Eigenvalues of B, respectively. The patient residing at minimum distance from the origin in the new coordinate space is considered the reference image. Given the reference image, all the remaining subjects in the atlas dataset were non-rigidly warped to the reference image. All these tasks are performed offline and at the end of this stage *(N-1=22)* transformation matrices *Tr(A,R)* mapping the atlas images (A) to the selected reference image (R), are available (Fig. 1: offline step). For the new target image (T), the reference image is non-rigidly registered to it and the resulting transformation matrix *Tr(R,T)* is combined with the pre-computed matrices *Tr(A,R)* to transform the entire atlas dataset to the target image (Fig. 1: online step). Thereafter, the arithmetic average (AA-ORMA) and voxel-wise weighting based on mean square intensity difference [7] (VWW-ORMA) atlas fusion approaches were utilized to generate the pseudo-CT images.

The performance of ORMA was compared with conventional atlas-based method consisting in direct registration of the entire atlas images to the target (Direct) followed by arithmetic average (AA-Direct) and voxel-wise weighting (VWW-Direct) atlas fusion schemes. The resulting attenuation maps were analyzed using the accuracy of extracted whole-body bone and SUV bias in PET images as metrics for evaluation.

$$DSC(C,P)=\frac{2|C\cap P|}{|C|+|P|}\quad RVD(C,P)=100\times\frac{|C|-|P|}{|P|}\quad MASD(C,P)=\frac{d_{ave}(S_C,S_P)+d_{ave}(S_P,S_C)}{2}$$

where C and P denote bone mask from CT and pseudo-CT images, respectively. $d_{ave}(S_C,S_P)$ computes the average direct surface distance from all points on the reference bone surface S_C to the segmented bone surface S_P.

Table 1. Comparison of various extracted bone accuracy validation metrics (mean±SD).

Method	DSC	RVD(%)	MASD (mm)
AA-Direct	0.60±0.02	-46.0±02.4	10.7±03.9
AA-ORMA	0.55±0.03	-52.6±02.5	11.3±03.6
VWW-Direct	0.82±0.04	-13.0±04.1	04.0±01.1
VWW-ORMA	0.76±0.05	-19.8±05.4	06.9±01.8

III. Results and Discussion

Pair-wise registration of the 23 images were carried out to acquire 253 transformation matrices required to fill up the symmetric 23×23 distance matrix D. MDS was performed to compute the 23 (number of atlas images) coordinates in 2 dimensions which were determined by considering the dramatic drop in computed Eigenvalues of the distance matrix. The image residing at the closest location to the origin was chosen to be the best reference image.

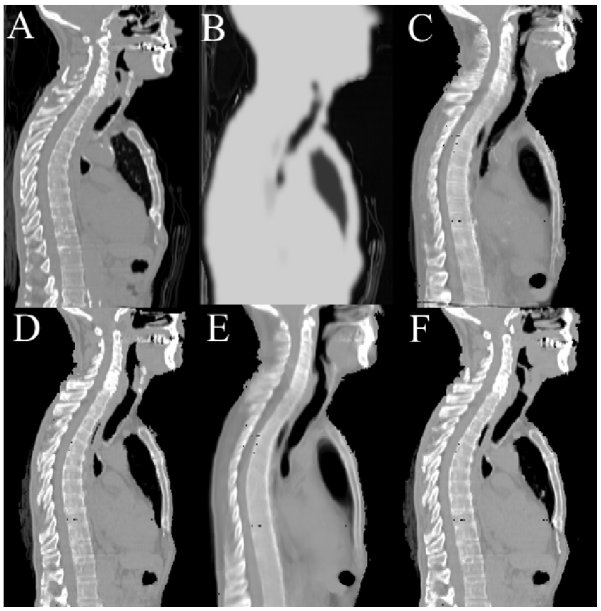

Fig 2. Representative slice of MR-derived attenuation maps. (A) Reference CT, (B) 3-class, (C) Average, (D) Voxel-wise weighting, (E) ORMA average and (G) ORMA voxel-wise weighting.

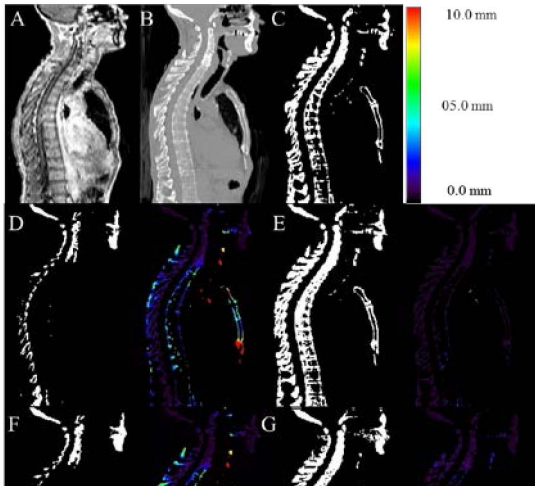

Fig 3. Representative slice of bone segmentation from MR image together with corresponding error distance map. (A) In-phase MR image, (B) corresponding CT image, (C) binary image of reference bone (extracted by a threshold of 180 HU), (D) Average, (E) Voxel-wise weighting, (F) ORMA average, (G) ORMA voxel-wise weighting.

Representative sagittal slices of created MR-derived pseudo-CT images are shown in figure 2. In addition to attenuation maps obtained from the atlas-based methods, the 3-class attenuation map generated by the Philips PET/MR scanner [8] is also incorporated in our analysis.

The sagittal slices were chosen for visual assessment of bone extraction accuracy and also the sharpness of lung and windpipe boundaries. The visual inspection of figure 2 reveals that averaging the atlas fusion method, whether applying direct registration (figure 2C) or ORMA approach (figure 2E), tends to produce remarkable amount of blurring and un-sharpness compared to VWW approaches whether utilizing direct atlas registration (figure 2D) or ORMA (figure 2F). Figure 3 depicts representative binary masks of extracted bone from the four pseudo-CT attenuation maps together with their corresponding error distance map calculated by taking the CT-derived bone (figure 3C) as reference.

Since delineation of bony structures is the foremost challenge in MR-guided AC, the pseudo-CT images were compared according to the accuracy of resolved bone (Table 1). VWW atlas fusion approaches show highly significant improvement for all validation measures compared to the AA fusion for both ORMA and direct registration approaches. However, a relatively modest loss in accuracy is observed when using the ORMA approach, which is a reasonable compromise.

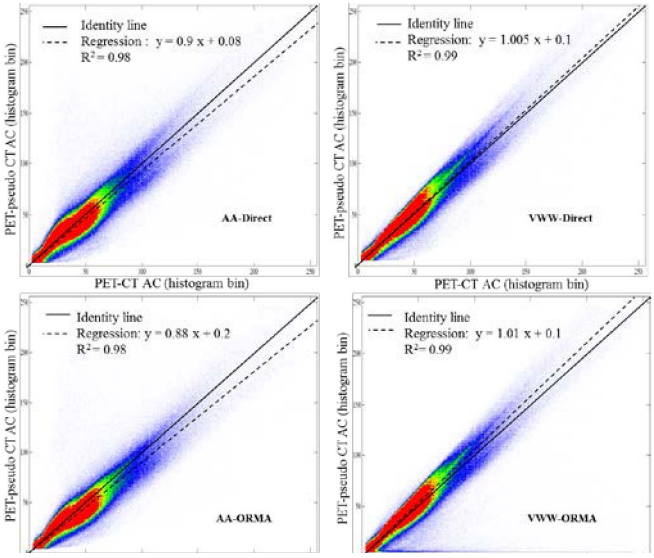

Fig 4. Joint histograms of PET images corrected for attenuation using pseudo-CTs correlated with those corrected using reference CT images. Each histogram bin corresponds to 0.06 SUV.

Figure 4 depicts the joint histogram graphs obtained from plotting the intensity correlation between different MRI-guided attenuation maps and the corresponding CT images. VWW atlas fusion yielded the highest correlation (y=1.02x+0.2 and R^2= 0.99) while the ORMA approach produced lower correlation compared to the direct atlas registration framework. The same trend is seen in figure 5 where the joint histograms of PET voxel intensities are plotted. Exploiting the ORMA approach as an alternative to direct atlas registration engendered trivial deviation from actual activity measured on PET/CT images. However, the time required by the VWW-ORMA approach was 20 times faster than that of VWW-Direct.

IV. Conclusions

We have demonstrated that the proposed method is capable of generating decent PET attenuation maps with a Dice similarity of 0.76±0.05 for extraction of bony structures. This is in contrast to the conventional atlas-based method, which results in a Dice similarity of 0.82±0.04 at the expense of substantial increase in computation time since *N* (number of atlas images) image registrations are required. The quantitative analysis of PET images also revealed good correlation between PET images corrected for attenuation using the proposed approach and reference CT images. Despite a modest lower performance, the processing time for atlas-based pseudo-CT generation is significantly reduced (a factor *N*).

Acknowledgements

This work was supported by the Swiss National Science Foundation under grant SNSF 31003A-149957.

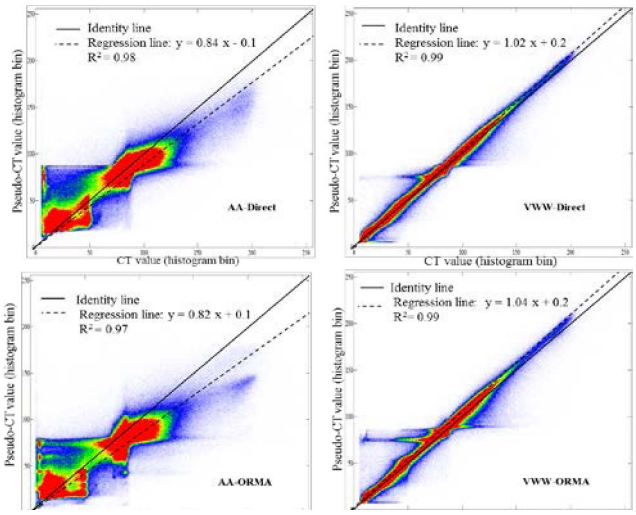

Fig 5. Joint histograms of pseudo-CTs correlated with reference CT. Each histogram bin corresponds to 16 HUs.

References

[1] H. Arabi and H. Zaidi, "Comparison of atlas-based bone segmentation methods in whole-body PET/MRI," *IEEE Nuclear Science Symposium & Medical Imaging Conference,* vol. Seattle, USA, 2014.

[2] I. Bezrukov, F. Mantlik, H. Schmidt, B. Scholkopf, and B. J. Pichler, "MR-based PET attenuation correction for PET/MR imaging.," *Semin Nucl Med,* vol. 43, pp. 45-59, 2013.

[3] N. J. Tustison, B. B. Avants, P. A. Cook, Y. Zheng, A. Egan, P. A. Yushkevich, *et al.*, "N4ITK: improved N3 bias correction.," *IEEE Trans Med Imaging,* vol. 29, pp. 1310-1320, 2010.

[4] F. L. Bookstein, "Principal warps: Thin-plate splines and the decomposition of deformations," *IEEE Trans Pattern Analy Machine Intell,* vol. 11, pp. 567-585, 1989.

[5] H. Park, P. Bland, A. Hero, and C. Meyer, "Least biased target selection in probabilistic atlas construction," *Medical Image Computing and Computer-Assisted Intervention–MICCAI,* pp. 419-426, 2005.

[6] S. Klein, M. Staring, K. Murphy, M. A. Viergever, and J. P. W. Pluim, "elastix: A toolbox for intensity-based medical image registration.," *IEEE Trans Med Imaging,* vol. 29, pp. 196-205, 2010.

[7] X. Artaechevarria, A. Munoz-Barrutia, and C. Ortiz-de-Solorzano, "Combination strategies in multi-atlas image segmentation: application to brain MR data.," *IEEE Trans Med Imaging,* vol. 28, pp. 1266-1277, 2009.

[8] H. Zaidi, N. Ojha, M. Morich, J. Griesmer, Z. Hu, P. Maniawski, *et al.*, "Design and performance evaluation of a whole-body Ingenuity TF PET-MRI system.," *Phys Med Biol,* vol. 56, pp. 3091-3106, 2011.